Human Molecular Genetics, 2017, Vol. 26, No. 14 2719–2731

doi: 10.1093/hmg/ddx159
Advance Access Publication Date: 25 April 2017
Original Article

ORIGINAL ARTICLE

Hepatic Tm6sf2 overexpression affects cellular ApoB-trafficking, plasma lipid levels, hepatic steatosis and atherosclerosis

Nicole Ehrhardt[1], Michael E. Doche[2], Shuang Chen[2,3,4], Hui Z. Mao[1], Meghan T. Walsh[5], Candy Bedoya[1], Maha Guindi[6], Weidong Xiong[7], Joseph Ignatius Irudayam[7], Jahangir Iqbal[5], Sebastien Fuchs[1], Samuel W. French[8,9,10], M. Mahmood Hussain[5,11], Moshe Arditi[2,3,4,12], Vaithilingaraja Arumugaswami[7,13] and Miklós Péterfy[1,2,14,*]

[1]Department of Basic Medical Sciences, Western University of Health Sciences, Pomona, CA 91766, USA, [2]Department of Biomedical Sciences, [3]Department of Pediatrics, [4]Infectious and Immunologic Diseases Research Center, Cedars-Sinai Medical Center, Los Angeles, CA 90048, USA, [5]Department of Cell Biology, SUNY Downstate Medical Center, Brooklyn, NY 11203, USA, [6]Department of Pathology and Laboratory Medicine, [7]Board of Governors Regenerative Medicine Institute, Cedars-Sinai Medical Center, Los Angeles, CA 90048, USA, [8]Department of Pathology and Laboratory Medicine, [9]Jonsson Comprehensive Cancer Center, [10]UCLA AIDS Institute, David Geffen School of Medicine at UCLA, Los Angeles, CA 90095, USA, [11]Winthrop-University Hospital, Mineola, NY 11501, USA, [12]Department of Pediatrics, [13]Department of Surgery and [14]Department of Medicine, David Geffen School of Medicine at UCLA, Los Angeles, CA 90095, USA

*To whom correspondence should be addressed at: Department of Basic Medical Sciences, Western University of Health Sciences, 309 E. Second St., HEC 2212, Pomona, CA 91766, USA. Tel: +1 9097063949; Fax: +1 9094695698; E-mail: mpeterfy@westernu.edu

Abstract

The human transmembrane 6 superfamily member 2 (*TM6SF2*) gene has been implicated in plasma lipoprotein metabolism, alcoholic and non-alcoholic fatty liver disease and myocardial infarction in multiple genome-wide association studies. To investigate the role of Tm6sf2 in metabolic homeostasis, we generated mice with elevated expression using adeno-associated virus (AAV)-mediated gene delivery. Hepatic overexpression of mouse Tm6sf2 resulted in phenotypes previously observed in Tm6sf2-deficient mice including reduced plasma lipid levels, diminished hepatic triglycerides secretion and increased hepatosteatosis. Furthermore, increased hepatic Tm6sf2 expression protected against the development of atherosclerosis in LDL-receptor/ApoB48-deficient mice. In cultured human hepatocytes, Tm6sf2 overexpression reduced apolipoprotein B secretion and resulted in its accumulation within the endoplasmic reticulum (ER) suggesting impaired ER-to-Golgi trafficking of pre-very low-density lipoprotein (VLDL) particles. Analysis of two metabolic trait-associated coding polymorphisms in the human *TM6SF2* gene (rs58542926 and rs187429064) revealed that both variants impact TM6SF2 expression by affecting the rate of protein turnover. These data demonstrate that rs58542926 (E167K) and rs187429064 (L156P) are functional variants and suggest

Received: December 11, 2016. **Revised:** April 19, 2017. **Accepted:** April 21, 2017

that they influence metabolic traits through altered TM6SF2 protein stability. Taken together, our results indicate that cellular Tm6sf2 level is an important determinant of VLDL metabolism and further implicate *TM6SF2* as a causative gene underlying metabolic disease and trait associations at the 19p13.11 locus.

Introduction

Genome-wide association studies uncovered hundreds of chromosomal regions associated with metabolic traits and diseases in human populations. Plasma lipoprotein levels are determined by genetic variation at over 150 loci, most of which have not been implicated in lipid metabolism before (1). Thus, characterization of genes and polymorphisms underlying these loci may offer novel mechanistic insights into metabolic regulation and dysfunction.

One of the most widely replicated chromosomal regions associated with metabolic traits is the CILP2 (a.k.a. NCAN or PBX4) locus at 19p13.11, which has been linked to variation in fasting and postprandial plasma lipid levels, alcoholic and non-alcoholic fatty liver disease (NAFLD), type 2 diabetes and coronary artery disease (1–9). Of the more than dozen genes located within the 19p13.11 critical genomic interval, transmembrane 6 superfamily member 2 (*TM6SF2*) has emerged as a candidate for underlying metabolic trait associations at this locus. Genetic studies identified two missense single nucleotide polymorphisms (SNPs) in the *TM6SF2* gene, E167K (rs58542926) and L156P (rs187429064), as independent determinants of plasma cholesterol and triglycerides (TG) levels (3,5). Moreover, E167K has been linked with several NAFLD-related phenotypes including elevated liver enzymes, hepatic steatosis and fibrosis, as well as alcohol-induced cirrhosis and hepatocellular carcinoma (8,10–14).

TM6SF2 is predominantly expressed in tissues associated with the production of apolipoprotein B (APOB)-lipoproteins including liver, small intestine and kidney suggesting a potential role in lipoprotein metabolism (3). Indeed, mice with whole-body or liver-specific *Tm6sf2* deficiency exhibited low plasma and elevated hepatic lipid levels likely due to reduced hepatic TG secretion (3,15). Furthermore, *tm6sf2* loss-of-function in zebrafish leads to decreased low-density lipoprotein (LDL)-cholesterol and hepatic steatosis (9). Consistent with these studies, knock-down of *TM6SF2* in hepatoma cell lines suppressed TG-secretion and resulted in intracellular TG accumulation (16). However, studies in mouse models with elevated expression of *TM6SF2* produced conflicting results. Transgenic overexpression of *TM6SF2* using an albumin promoter was associated with excess hepatic lipid accumulation, similar to the effect of *Tm6sf2* deficiency (17). Furthermore, plasma TG levels were unaffected or decreased in *TM6SF2* transgenic mice on chow or high-fat diets, respectively, whereas adenoviral overexpression resulted in elevated plasma lipids (2,17). Thus, while its involvement in lipid metabolism is now well established, the role of *TM6SF2* expression in the regulation of plasma and hepatic lipid traits is incompletely understood.

TM6SF2 is a multi-pass membrane protein localized to the endoplasmic reticulum (ER) and ER-Golgi intermediate compartment (ERGIC) (3,15). On the basis of sequence similarity to Emopamil-binding protein, an enzyme with sterol isomerase activity, TM6SF2 has been hypothesized to play a role in sterol biosynthesis (18) and a recent study provided experimental evidence consistent with this hypothesis (17). Alternatively, it has been proposed that Tm6sf2 is involved in the transfer of neutral lipids from cytoplasmic to luminal lipid droplets or very low-density lipoprotein (VLDL) particles (15). Although its exact molecular function remains to be established, Tm6sf2 has emerged as a novel player in cellular lipoprotein metabolism.

Genetic studies identified two missense SNPs in the *TM6SF2* gene, E167K (rs58542926) and L156P (rs187429064), as independent determinants of plasma cholesterol and TG levels (3,5). E167K has also been linked with several NAFLD-related phenotypes including elevated liver enzymes, hepatic steatosis and fibrosis, as well as alcohol-induced cirrhosis and hepatocellular carcinoma (8,13–17). The E167K amino acid change reduced expression of TM6SF2 protein in a previous study, but the underlying mechanism has not been investigated (3). The potential functional impact of L156P polymorphism remains undetermined.

In the present study we generated and characterized mouse and *in vitro* models to assess the physiological and cellular impact of *Tm6sf2* overexpression on lipoprotein metabolism and related traits. Furthermore, we investigated the molecular mechanism through which human E167K and L156P polymorphisms affect TM6SF2 expression.

Results

Hepatic overexpression of Tm6sf2 suppresses plasma lipid levels

While the plasma lipid-lowering effect of hepatic Tm6sf2 deficiency has previously been demonstrated (2,3,15), the metabolic impact of elevated Tm6sf2 expression remains unclear. To investigate this issue, we employed adeno-associated virus (AAV)-mediated gene delivery using an AAV8 vector harboring the mouse *Tm6sf2* cDNA driven by the thyroxine-binding globulin (TBG) promoter, which allows hepatocyte-specific expression of the transgene (19). Relative to mice injected with empty vector (AAV-Null), mice receiving AAV-Tm6sf2 (10^{12} gc/mouse) unexpectedly exhibited lower levels of plasma lipids including TG and cholesterol associated with both high-density lipoprotein (HDL) and non-HDL lipoproteins (Fig. 1A). These differences reflect 40–60% suppression of plasma lipid concentrations in AAV-Tm6sf2-injected mice compared with pre-injection levels, whereas plasma lipids remained unchanged after AAV-Null injection (Supplementary Material, Fig. S1A). Suppression of lipid levels by AAV-Tm6sf2 was sustained for up to 12 weeks following virus injection (Supplementary Material, Fig. S1B). Lipoprotein separation by fast-performance liquid chromatography (FPLC) indicated that Tm6sf2 overexpression reduced TG content in the VLDL and LDL fractions, as well as cholesterol associated with the VLDL, LDL and HDL fractions (Fig. 1B).

In light of previous studies in *Tm6sf2*-deficient mice the lipid-lowering effect of Tm6sf2 overexpression was paradoxical, therefore we investigated experimental parameters that may have impacted our results. As the AAV dose used in initial experiments [10^{12} genome copies (gc) per mouse] produced >100-fold elevated hepatic *Tm6sf2* expression over endogenous levels (Supplementary Material, Fig. S1C), we assessed the effects of more moderate overexpression. Two weeks after AAV injection, plasma alanine aminotransferase

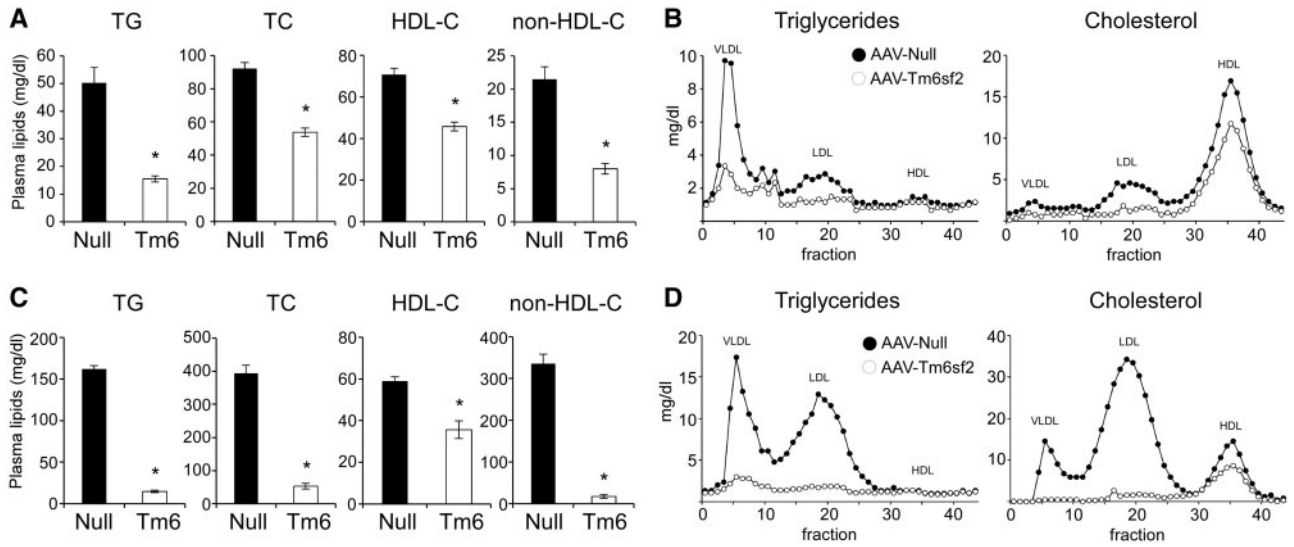

Figure 1. Hepatic Tm6sf2 overexpression is associated with reduced plasma lipid levels, hepatic steatosis and inflammatory gene expression. Eight-week-old male C57BL/6J (**A** and **B**) or Ldlr$^{-/-}$;ApoB$^{100/100}$ (**C** and **D**) mice were injected with empty (Null) or Tm6sf2-expressing (Tm6) AAV (1×10^{12} gc/mouse) and maintained on chow diet. (A) Plasma lipid levels in C57BL/6J mice 2 weeks after virus injection ($n=8$ mice per group). (B) FPLC lipoprotein profiles of samples shown in (A) (pooled plasma from eight mice per group). (**C**) Plasma lipid levels in hypercholesterolemic Ldlr$^{-/-}$;ApoB$^{100/100}$ mice 4 weeks after AAV injection ($n=3$ mice per group). (**D**) FPLC lipoprotein profiles of samples shown in (**C**) (pools of three mice per group). Data are shown as the mean ± SEM. *$P<0.05$ by Student's *t*-test.

(ALT) activity remained unchanged even with the highest dose (10^{12} gc/mouse) of virus (Fig. 2C). Moreover, lowering the dose of AAV from 10^{12} to 10^{10} gc/mouse reduced the percent of hepatocytes transduced (Supplementary Material, Fig. S1C) and the degree of hepatic Tm6sf2 overexpression (Supplementary Material, Fig. S1D), and gradually diminished the suppressive effect on plasma lipid levels in a dose-dependent manner (Supplementary Material, Fig. S1E). At a nominal overexpression of 4-fold, the lipid-lowering effect of Tm6sf2 was undetectable likely due to low hepatocyte transduction efficiency at the corresponding AAV dose (i.e. 10^{10} gc/mouse). Feeding status (Supplementary Material, Fig. S1F) or administration of a high-fat diet (Supplementary Material, Fig. S1H) did not alter the impact of Tm6sf2 overexpression on plasma lipid levels. As Tm6sf2 is an ER membrane protein (15,16), we also considered the possibility that ER stress triggered by its overexpression may be responsible for the hypolipidemic phenotype in our mouse model. However, hepatic transcript levels of genes associated with the unfolded protein response (UPR) remained unchanged in AAV-Tm6sf2 mice (Supplementary Material, Fig. S1G). In conclusion, our results demonstrate that elevated hepatic expression of Tm6sf2 suppresses plasma TG and cholesterol levels.

To investigate whether Tm6sf2 overexpression protects against genetically induced hyperlipidemia, we injected AAV-Tm6sf2 (10^{12} gc/mouse) in Ldlr$^{-/-}$;ApoB$^{100/100}$ double knock-out (DKO) mice deficient in LDL-receptor and apolipoprotein B48 (ApoB48) (20). As expected, DKO mice injected with control virus exhibited hypercholesterolemia in the VLDL and LDL plasma fractions of both males (Fig. 1C and D) and females (Supplementary Material, Fig. S1I and J). Administration of AAV-Tm6sf2 markedly reduced plasma TG and cholesterol levels in non-HDL fractions and completely normalized hypercholesterolemia in DKO mice (Fig. 1C and D; Supplementary Material, Fig. S1I–K). These results confirm the lipid-lowering effect of AAV-Tm6sf2 observed in wild-type mice and demonstrate that Tm6sf2 overexpression affects plasma cholesterol levels through an LDL-receptor (Ldlr)-independent mechanism.

Overexpression of human TM6SF2 isoform is associated with transient plasma lipid phenotypes and hepatic injury

In contrast to our results with mouse Tm6sf2, adenoviral overexpression of human TM6SF2 has previously been reported to elevate plasma TG and cholesterol levels (2). To identify the source of conflict between studies, we evaluated the impact of human and mouse Tm6sf2 on plasma lipid phenotypes by performing a side-by-side comparison of the isoforms using identical AAV doses (i.e. 10^{12} gc/mouse). Consistent with our previous results, injection of AAV-Tm6sf2 robustly and persistently lowered lipid levels, but the effect of AAV-TM6SF2 administration was transient and undetectable 4 weeks after injection (Fig. 2A). While TM6SF2 modestly suppressed TG levels 2 weeks post-injection, it had no effect on total or HDL-cholesterol and, in sharp contrast to Tm6sf2, increased non-HDL-cholesterol (Fig. 2A). These results demonstrate that the impact of human and mouse Tm6sf2 overexpression on plasma lipid levels is markedly different. To investigate whether the observed phenotypic differences between Tm6sf2 isoforms were due to differences in transgene expression, we performed a time-course analysis. Whereas expression of human and mouse Tm6sf2 were similar 1 week after AAV injection, hepatic TM6SF2 mRNA levels dropped precipitously by 2 weeks, and by 4 weeks expression of the human isoform was less than 10% of Tm6sf2 (Fig. 2B). Moreover, 2 weeks after AAV injection TM6SF2, but not Tm6sf2, expression resulted in elevated plasma ALT activity (Fig. 2C) and direct bilirubin level (Fig. 2D), increased hepatic expression of the macrophage marker *Cd68* (Fig. 2E) and inflammatory cell infiltration (Supplementary Material, Fig. S2A). The inflammatory phenotype in AAV-TM6SF2 mice was not associated with elevated ER stress; in fact several markers of the UPR were suppressed by TM6SF2 expression (Supplementary Material, Fig. S2B). Taken together, these results suggest that acute overexpression of TM6SF2 triggers hepatitis and hepatic injury followed by the elimination of transduced cells. These data also raise the possibility that inflammation associated with TM6SF2 overexpression

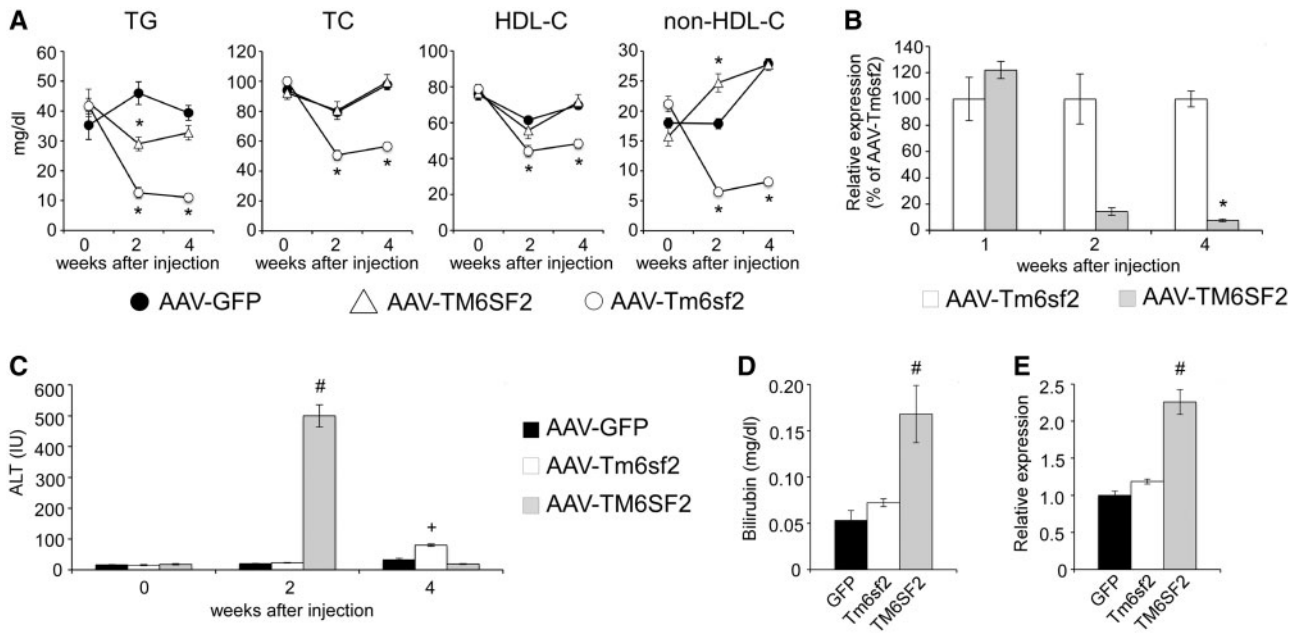

Figure 2. Hepatic overexpression of human TM6SF2, but not mouse Tm6sf2, is associated with liver injury and transient plasma lipid phenotypes. C57BL/6J male mice were injected with equal doses (1×10^{12} gc/mouse) of AAV-GFP, AAV-TM6SF2 and AAV-Tm6sf2 vectors. (**A**) Time-course of plasma lipid levels ($n=6$–8 mice per group). (**B**) Temporal changes in the hepatic expression of TM6SF2 relative to Tm6sf2 ($n=4$–5 mice per group). (**C**) Time-course of plasma ALT activity ($n=8$ mice per group). (**D**) Plasma direct bilirubin levels 2 weeks after AAV injection ($n=2$–4 mice per group). (**E**) Hepatic expression of *Cd68* 2 weeks after AAV injection ($n=2$–4 mice per group). Data are shown as the mean ± SEM. $^{*}P<0.05$ by Student's *t*-test; $^{\#}$ and ^{+}P (versus GFP) and *P* (versus TM6SF2) <0.05 by Kruskal–Wallis test followed by Dunn's post hoc test.

may confound its impact on plasma lipid phenotypes and provide a potential explanation for the conflict between our study and a previous report (2). We used the mouse Tm6sf2 isoform in all subsequent *in vivo* experiments.

Tm6sf2 overexpression suppresses VLDL-TG secretion and promotes steatosis and inflammatory gene expression

As Tm6sf2 has previously been implicated in hepatic TG secretion in deficiency models (3,15), we next investigated if Tm6sf2 overexpression also affects this process. Eight weeks after AAV injection (10^{12} gc/mouse), we measured the rate of TG accumulation in plasma in the presence of Pluronic F-127, an inhibitor of TG clearance. AAV-Tm6sf2 suppressed the rate of TG secretion by ~34% relative to control (Fig. 3A) pointing to diminished hepatic VLDL-TG secretion as the mechanism responsible for the plasma TG-lowering effect of Tm6sf2 overexpression. Interestingly, cholesterol secretion remained unchanged (Supplementary Material, Fig. S3A) suggesting that AAV-Tm6sf2 affected lipid composition of the VLDL particle.

While liver morphology was indistinguishable in control and AAV-Tm6sf2-injected mice, Oil Red O (ORO) staining revealed increased neutral lipid accumulation in the latter (Fig. 3B). Indeed, biochemical analysis demonstrated elevated hepatic TG content in AAV-Tm6sf2 mice, whereas hepatic cholesterol levels remained unaffected (Fig. 3C). Four weeks after virus injection Tm6sf2 overexpression was also associated with modest, but detectable, elevation of plasma ALT activity likely reflecting hepatic steatosis (Fig. 2C). The steatotic effect of AAV-Tm6sf2 was not due to transcriptional changes related to lipid metabolism, as expression of genes involved in fatty acid (FA) synthesis and oxidation, TG synthesis, cholesterol metabolism, and VLDL secretion remained unchanged (Supplementary Material, Fig. S3C). Moreover, functional assessment of microsomal triglyceride transfer protein (Mttp), the rate limiting enzyme in VLDL synthesis, revealed elevated activities in AAV-Tm6sf2 liver (Supplementary Material, Fig. S3D) demonstrating that altered Mttp function was not responsible for reduced VLDL-TG secretion in these mice. In addition to hepatic steatosis, genetic variation in the human TM6SF2 gene has also been linked to inflammation and fibrosis. Histopathological evaluation of AAV-Tm6sf2 livers failed to reveal abnormalities (ballooning, Mallory bodies, inflammation, fibrosis) commonly associated with steatohepatitis and cirrhosis (Fig. 3B; Supplementary Material, Fig. S3B). However, Tm6sf2 overexpression modestly induced expression of several markers of inflammation (Il1a, Il1b, Ccl2/Mcp1, Ccl7/Mcp3, Cxcl10/IP-10, Saa3) and genes involved in hepatic fibrogenesis (Col1a1, Col3a1, Timp1, Mmp2) (Fig. 3D). Collectively, our results suggest that Tm6sf2 overexpression likely suppresses VLDL-TG secretion through post-transcriptional mechanisms, which may include impaired VLDL assembly or intracellular trafficking, increased VLDL degradation, decreased *de novo* lipogenesis or elevated FA oxidation. Furthermore, we also established that Tm6sf2 overexpression promoted hepatic steatosis and increased inflammatory and fibrogenic gene expression.

Hepatic Tm6sf2 overexpression protects against coronary artery disease

The dramatic LDL-cholesterol-lowering effect of AAV-Tm6sf2 prompted us to test whether hepatic Tm6sf2 overexpression may protect against coronary artery disease. To test this hypothesis, we fed a high-cholesterol (HC) diet to DKO mice injected with AAV-Null or AAV-Tm6sf2 vectors (10^{12} gc/mouse)

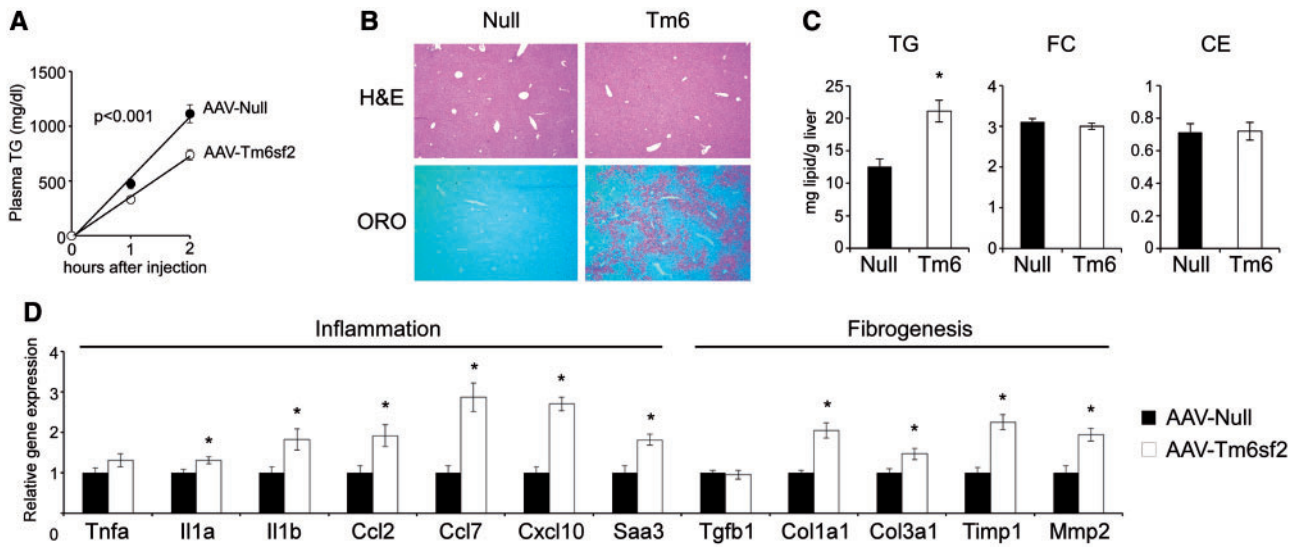

Figure 3. Hepatic Tm6sf2 overexpression is associated with decreased VLDL-TG secretion, hepatic steatosis and inflammatory gene expression. (A) Hepatic TG secretion 8 weeks after AAV injection (1×10^{12} gc/mouse) following Pluronic F-127 administration (0 h) to inhibit TG clearance ($n=4$–5 mice per group). (B) Representative H&E and Oil Red O (ORO)-stained liver sections 12 weeks after virus injection. (C) Hepatic triglyceride (TG), free cholesterol (FC) and cholesterol ester (CE) concentrations 12 weeks after AAV injection ($n=5$–8 mice per group). (D) Hepatic mRNA expression of genes involved in inflammation and fibrogenesis 12 weeks after AAV injection ($n=5$–8 mice per group). Data are shown as the mean ± SEM. *$P<0.05$ by Student's *t*-test or two-factor ANOVA (A).

and assessed atherosclerotic lesions (Fig. 4A). After 12 weeks on the HC diet, AAV-Tm6sf2-injected mice demonstrated significantly lower plasma TG (88% reduction) and cholesterol (72% reduction) levels associated with ApoB-lipoproteins, but elevated HDL-cholesterol concentrations (35% increase) relative to AAV-Null controls (Fig. 4B and 4C). Visual inspection of the aortic arch revealed massive lipid deposition in control mice, whereas AAV-Tm6sf2 aortas were largely devoid of atherosclerotic plaques (Fig. 4D). Morphometric analysis of histological sections confirmed substantially reduced lesion area and ORO-stained area in the aortic arch (Fig. 4E), whole aorta (Fig. 4F) and aortic sinus (Fig. 4G) of AAV-Tm6sf2 mice. These results indicate that suppression of plasma cholesterol levels by Tm6sf2 overexpression protects against atherosclerosis in DKO mice.

Tm6sf2 overexpression suppresses APOB secretion and leads to its accumulation in the ER

Our *in vivo* results indicated that overexpression of Tm6sf2 reduced plasma lipid levels by diminishing the hepatic secretion of TG. To investigate the cellular mechanisms underlying this effect, we assessed the impact of Tm6sf2 overexpression on APOB metabolism in human hepatocytes. High-level overexpression of Tm6sf2 (Supplementary Material, Fig. S4A) strongly suppressed the secretion of APOB, but not albumin, into the culture media of Huh7 cells (Fig. 5A). Similar results were obtained in a Huh7 cell line with more moderate levels of Tm6sf2 expression (Supplementary Material, Fig. S4B) and in primary human hepatocyte-like cells (HLCs) differentiated from induced pluripotent stem cells (iPSC) (Supplementary Material, Fig. S4C). Furthermore, reduced lipoprotein secretion was associated with modest, but significant elevations of intracellular TG, whereas cholesterol content remained unchanged (Fig. 5B). Consistent with *in vivo* observations, excess Tm6sf2 did not significantly affect the expression of genes involved in cellular FA, TG and VLDL metabolism or ER stress, although minor decreases in HMG-CoA synthase (HMGCS1) and HMG-CoA reductase (HMGCR) mRNA levels were detected (Supplementary Material, Fig. S4D).

To account for reduced APOB secretion in Tm6sf2-overexpressing cells, we considered the possibility that Tm6sf2 overexpression promotes intracellular APOB degradation, a principal process in the regulation of VLDL secretion. As limited TG availability within the ER is one of the key mechanisms triggering APOB degradation, we attempted to rescue the secretion defect in Tm6sf2-overexpressing cells by oleic acid (OA) supplementation, a treatment known to promote APOB lipidation and secretion (21). As expected, OA treatment stimulated APOB secretion in both control and Tm6sf2-overexpressing Hep3B cells, but it failed to mitigate the inhibitory effect of Tm6sf2 overexpression (Fig. 5C, left panel). Furthermore, MTTP activity was unaffected by Tm6sf2 overexpression (Supplementary Material, Fig. S4E) suggesting that reduced APOB secretion was not due to impaired lipidation of nascent APOB in these cells. Next, we tested whether increased intracellular degradation of APOB played a role in the effect of Tm6sf2 overexpression on APOB secretion. Treatment with inhibitors of proteasomal (lactacystin) or autophagy (3-methyladenine) pathways of APOB degradation increased its secretion in both control and Tm6sf2-overexpressing cells (Fig. 5C, right panel). However, neither treatment abolished the inhibitory effect of Tm6sf2 overexpression demonstrating that reduced APOB secretion was not due to increased APOB degradation. Indeed, intracellular APOB levels were 2–3-fold elevated in Huh7 cells overexpressing Tm6sf2 and similar results were observed in HepG2 cells (Fig. 5D). Consistent with these *in vitro* observations, ApoB-100 and ApoB-48 levels were significantly lower in plasma (Fig. 5E), whereas the latter showed marked accumulation in the liver of AAV-Tm6sf2 mice (Fig. 5F).

To identify the cellular compartment of APOB accumulation in Tm6sf2-overexpressing cells, we performed sub-cellular localization studies using confocal immunofluorescence microscopy. Previous studies in rat hepatocytes demonstrated that at

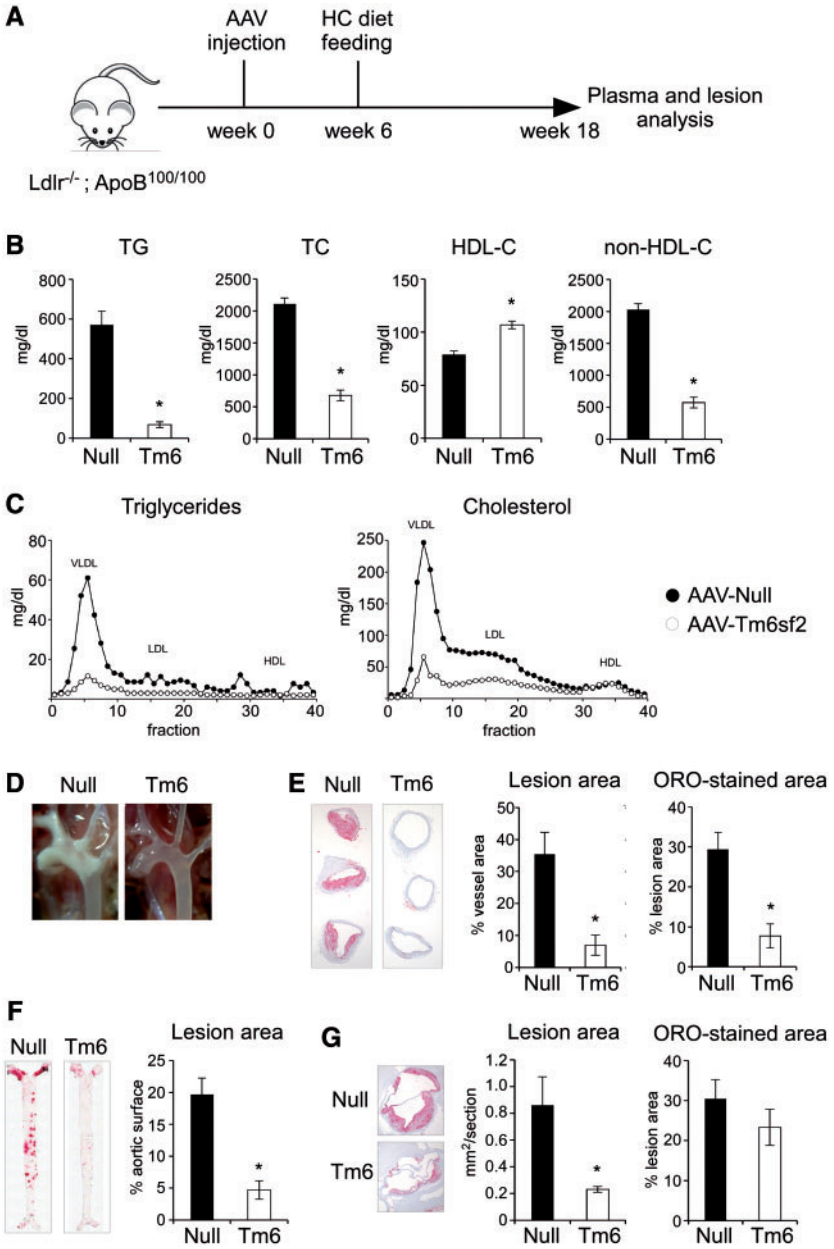

Figure 4. Hepatic Tm6sf2 overexpression protects against atherosclerosis. (**A**) Experimental design. Twelve-week-old Ldlr$^{-/-}$;ApoB100/100 mice were injected with empty (Null) or Tm6sf2-expressing (Tm6) AAV (1×10^{12} gc/mouse) and placed on a high-cholesterol (HC, 0.2% cholesterol) diet 6 weeks later. Plasma and lesion analyses were performed after 12 weeks of HC diet feeding. (**B**) Plasma lipid levels ($n=4$–5 per group). (**C**) FPLC lipoprotein profiles of samples shown in A (pooled plasma from four to five mice per group). (**D**) Photographs of exposed aortic arches and great vessels. (**E**) Left panels show representative aortic arch sections stained with ORO. Quantification of lesion sizes and ORO-stained area are shown on the right ($n=4$–5 mice per group). (**F**) Representative images of ORO-stained *en face* aorta preparations and quantification of aortic lesion coverage ($n=4$–5 mice per group). (**G**) Photomicrograph and quantification of aortic sinus lesion size and ORO-stained area ($n=4$–5 mice per group). Data are shown as the mean ± SEM. *$P<0.05$ by Student's *t*-test.

steady state cellular APOB is predominantly localized to the Golgi (22,23). In line with these results, APOB exhibited punctate staining pattern and only partial co-localization with calreticulin (CRT), an ER marker, in control Huh7 cells (Fig. 5G, upper panels). In contrast, cells overexpressing Tm6sf2 showed predominantly perinuclear staining of APOB and a high degree of co-localization with CRT demonstrating that APOB accumulated within the ER (Fig. 5G, lower panels). Taken together, these results suggest that Tm6sf2 overexpression suppresses cellular APOB secretion by interfering with the ER-to-Golgi transport of APOB-lipoprotein particles.

Metabolic trait-associated polymorphisms reduce TM6SF2 protein expression by increasing protein turnover

Exome-wide association studies identified two coding SNPs, rs187429064 (L156P) and rs58542926 (E167K), in the human TM6SF2 gene to be associated with plasma lipid levels and NAFLD (3,5). While the common alleles (L156 and E167) are evolutionarily conserved and the rare alleles (P156 and K167) are predicted to be deleterious, their impact on TM6SF2 remains largely uncharacterized. To address this question, we developed

Huh7 cell lines that stably express TM6SF2 isoforms representing the common and rare alleles of each polymorphism. Despite slightly elevated (P156) or similar (K167) mRNA levels (Fig. 6A), protein expression of both rare TM6SF2 isoforms was markedly reduced relative to the common (L156/E167) isoform (Fig. 6B). To investigate whether P156 or K167 affects TM6SF2 turnover, we assessed the degradation of luciferase-TM6SF2 fusion proteins in the presence of the protein synthesis inhibitor, cycloheximide (CHX). Consistent with their reduced steady-state expression, the P156 and K167 isoforms exhibited significantly increased rate of degradation ($t_{1/2}$ ~4.5 h) compared with common isoform ($t_{1/2}$ ~9 h) (Fig. 6C). These results demonstrate that rs58542926 and rs187429064 are functional variants at the 19p13.11 locus and affect TM6SF2 protein expression through altering its rate of turnover.

Discussion

In the present work, we employed mouse and *in vitro* models to investigate the role of Tm6sf2 in organismal and cellular lipid metabolism. We demonstrated that hepatic overexpression of Tm6sf2 lowers plasma lipid levels in wild-type and genetically hyperlipidemic mice, protects against atherosclerosis, and causes hepatic steatosis. Using cultured hepatocytes we established that Tm6sf2 overexpression suppresses ApoB-lipoprotein secretion through affecting intracellular lipoprotein trafficking. Collectively, our results indicate that Tm6sf2 expression level is an important determinant of cellular and organismal ApoB-lipoprotein metabolism and associated morbidities.

Strikingly, the metabolic constellation observed in Tm6sf2-overexpressing mice recapitulates the phenotypic consequences of Tm6sf2 deficiency and suggests that AAV-Tm6sf2 mice characterized in our study in fact represent a loss-of-function model. While this conclusion is unexpected, examples of phenocopy between overexpression and deficiency models have been documented and often involve proteins that are part of multiprotein complexes whose function is disrupted by stoichiometric imbalance (24,25). Thus, we hypothesize that Tm6sf2 function depends on interactions with other proteins, and both excess and deficiency of Tm6sf2 may interfere with the formation of a molecular complex required for normal cellular function. Identification of Tm6sf2-interacting proteins and better understanding of its molecular function will be required to substantiate this hypothesis.

The TM6SF2 chromosomal region is associated with plasma TG and cholesterol levels in multiple human populations (2,3,5) and AAV-Tm6sf2 mice reflected these phenotypes. Tm6sf2 overexpression markedly reduced plasma TG levels by suppressing hepatic VLDL-TG production. Tm6sf2 overexpression suppressed plasma ApoB levels in mice and diminished APOB secretion in hepatocytes *in vitro* suggesting that reduced VLDL particle secretion may be the underlying mechanism. However, as hepatic ApoB release was not directly assessed in our study, we cannot exclude the possibility of impaired VLDL lipidation as the cause of reduced VLDL-TG secretion, as has been reported in Tm6sf2-deficient mice (15). In fact, our observation that the rate of VLDL-cholesterol secretion remained unaffected in AAV-Tm6sf2 mice is consistent with the latter possibility. Clearly, further studies will be required to clarify the molecular mechanisms responsible for impaired hepatic TG secretion in the context of Tm6sf2 overexpression. AAV-Tm6sf2 mice also exhibited lower non-HDL (i.e. VLDL and LDL) cholesterol levels, which is a likely reflection of reduced ApoB-lipoprotein particle number in the circulation. Interestingly, HDL-cholesterol was also diminished in AAV-Tm6sf2 mice. As TG-rich lipoproteins play a role in HDL maturation (26,27), we hypothesize that this phenotype is a consequence of reduced ApoB-lipoprotein availability in AAV-Tm6sf2 mice. Taken together, the plasma lipid phenotypes in AAV-Tm6sf2 mice are similar to those observed in Tm6sf2 knock-out and knock-down mice (3,15) indicating that excess Tm6sf2 resulted in functional deficiency of the corresponding molecular pathway in our mouse model.

A previous study reported elevated plasma TG and cholesterol levels after adenoviral overexpression of human TM6SF2 (2). As this observation is in direct conflict with our results, we investigated the impact of several experimental parameters differing between the studies. We determined that the use of different Tm6sf2 isoforms (i.e. human versus mouse) for transgene expression is the likely source of discordant results. Side-by-side comparisons revealed that expression of the human, but not mouse, isoform resulted in hepatitis and liver injury likely reflecting immunogenicity of the human protein. Thus, plasma lipid phenotypes associated with the overexpression of human TM6SF2 may have been confounded by effects of hepatic inflammation, a pathology known to elevate TG and cholesterol levels (28,29).

Genetic variation in the human TM6SF2 gene is associated with pathological features of NAFLD including steatosis, steatohepatitis and fibrosis (2,3,10,12,13). AAV-Tm6sf2 mice recapitulated early aspects of the NAFLD pathology including hepatic lipid accumulation and elevated plasma ALT levels. Hepatic accumulation of neutral lipids has also been reported in Tm6sf2-deficient mouse models (3,15) providing further support to the idea that Tm6sf2 overexpression leads to loss-of-function phenotypes. As in Tm6sf2 deficiency, overexpression had no detectable transcriptional impact on genes involved in lipid biosynthesis, uptake or oxidation. Although we cannot exclude post-transcriptional effects on these processes, our results suggest that steatosis in AAV-Tm6sf2 mice is due, at least in part, to reduced hepatic VLDL-TG export. In contrast to genes involved in lipid homeostasis, Tm6sf2 overexpression resulted in the upregulation of several markers of inflammation and fibrogenesis 12 weeks after virus injection, although histological signs of hepatitis and fibrosis could not be detected at this timepoint. Thus, AAV-Tm6sf2 mice represent a novel model for the development of initial stages of NAFLD. Dietary manipulations and/or the use of susceptible genetic backgrounds in future studies may allow extension of the model to more advanced stages of the disease.

Through the characterization of $Ldlr^{-/-}$;$ApoB^{100/100}$ (DKO) mice, we demonstrated for the first time the role of Tm6sf2 in atherosclerosis. Our results suggest that Tm6sf2 exerts its effect through the modulation of atherogenic (i.e. ApoB-containing) lipoproteins and may be responsible for the association of corresponding chromosomal region with myocardial infarction in human populations (2). Notably, the impact of Tm6sf2 overexpression on plasma TG and cholesterol levels is more pronounced in DKO (80–90% reduction) than wild-type (50–60% reduction) mice. The dramatic reduction in plasma lipids in DKO mice may be due to upregulation of Ldlr-independent pathways of ApoB-lipoprotein clearance (30–32). Alternatively, as DKO mice express ApoB-100, but not ApoB-48, our results may suggest that the metabolism of ApoB-100-containing lipoproteins is more dependent on Tm6sf2 function than that of ApoB-48. Interestingly, differential effects of Tm6sf2 on ApoB isoforms have also been documented in Tm6sf2-deficient mice, which exhibit elevated hepatic secretion and plasma levels of ApoB-48, but not ApoB-100 (15). Taken together, these results

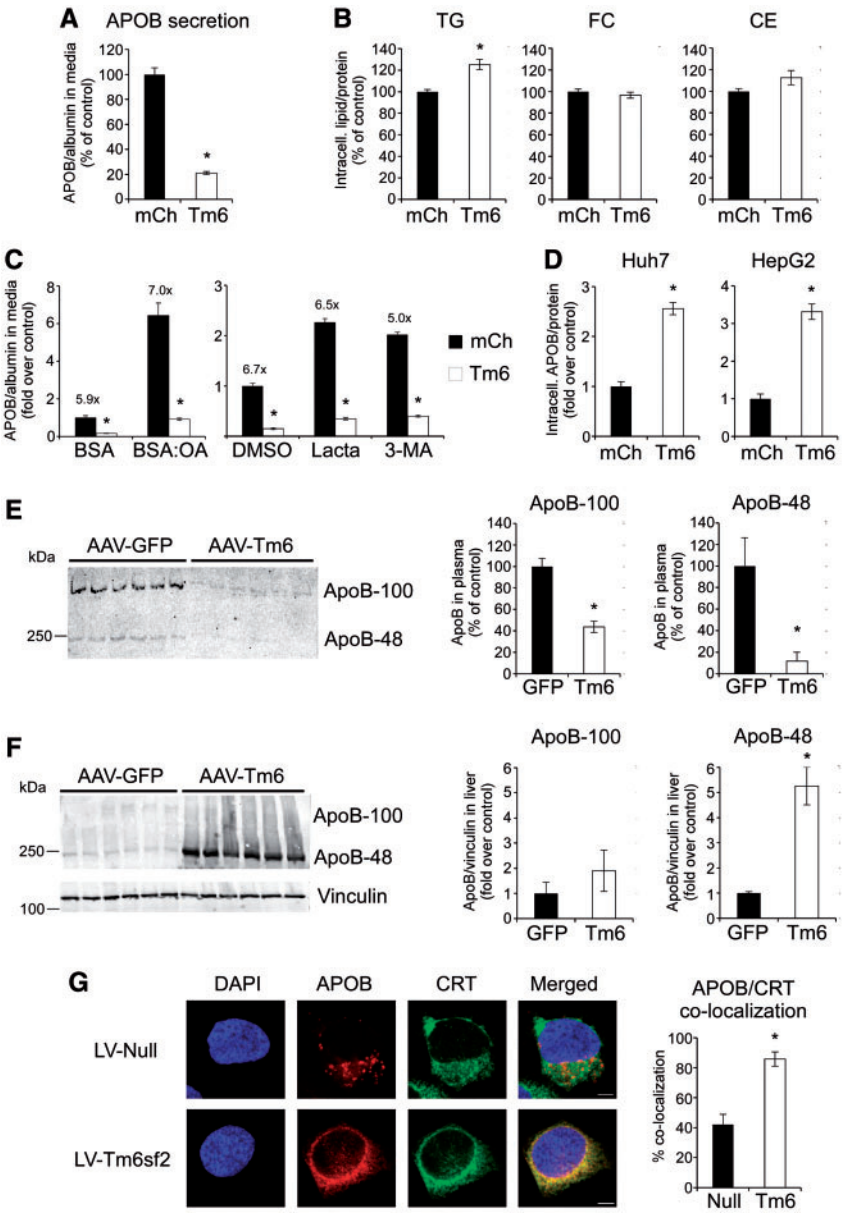

Figure 5. Tm6sf2 overexpression suppresses APOB secretion and leads to APOB-accumulation in the ER. Hepatoma cell lines were transduced with lentiviral (**A**, **B**, **D** and **G**) or adenoviral (**C**) vectors expressing mCherry (mCh), Tm6sf2 (Tm6) or no protein (Null). (A) Secretion of APOB into culture media by Huh7 cells stably expressing mCh or Tm6. Secreted APOB mass was normalized by concomitantly secreted albumin mass ($n = 3$ wells per group). (B) Intracellular lipid levels in Huh7 cells ($n = 3$–6 wells per group). (C) APOB secretion by Hep3B cells infected with mCh or Tm6 adenovirus and treated with oleic acid (OA, 0.6 mM) complexed to BSA (BSA:OA), lactacystin (Lacta, 10 μM) or 3-methyladenine (3-MA, 5 mM). APOB secretion was normalized by albumin and is presented as fold increase over control treatments (BSA or DMSO) of mCherry-expressing cells ($n = 3$ wells per group). Numbers above solid bars show the mCh/Tm6 APOB secretion ratio to indicate the effect of Tm6sf2 overexpression. (D) Intracellular APOB levels in Huh7 and HepG2 cells stably expressing mCherry or Tm6sf2 ($n = 6$ wells per group). (**E**) Plasma ApoB levels in mice infected with AAV-Tm6 or control AAV-GFP virus. Immunoblot analysis was performed using equal volumes of plasma samples obtained from six mice per group. Panels on the right show quantification of band intensities. (**F**) Hepatic ApoB levels in mice infected with AAV-Tm6 or control AAV-GFP virus. Immunoblot analysis was performed with anti-ApoB (top panel) or anti-vinculin antibody (lower panel). Panels on the right show quantification of normalized ApoB band intensities. (**G**) Subcellular localization of APOB (red) and calreticulin (CRT, green) in Huh7 cells by confocal immunofluorescence microscopy. Panel on the right shows the degree of co-localization between APOB and CRT as the fraction of pixels with coincident signals from both red and green channels ($n = 5$ fields per group and a total of 23–31 cells per group). Data are shown as the mean ± SEM. *$P < 0.05$ by Student's *t*-test.

suggest that Tm6sf2 functionally interacts with ApoB-lipoproteins in an isoform-specific manner. Identification of the underlying mechanisms in future studies may shed new light on the molecular function of Tm6sf2.

Under physiological conditions, VLDL secretion is principally regulated by pathways mediating the intracellular degradation of ApoB (33,34). However, it is clear that increased degradation is not responsible for impaired ApoB secretion in the context of Tm6sf2 overexpression, as cellular ApoB protein levels are not reduced, but in fact elevated in liver as well as in cultured hepatocytes. The cellular accumulation of ApoB implies that initial lipidation of the protein is not impaired in cells overexpressing Tm6sf2. Moreover, our observation that ApoB is trapped within the ER of these cells indicates that excess Tm6sf2 interferes

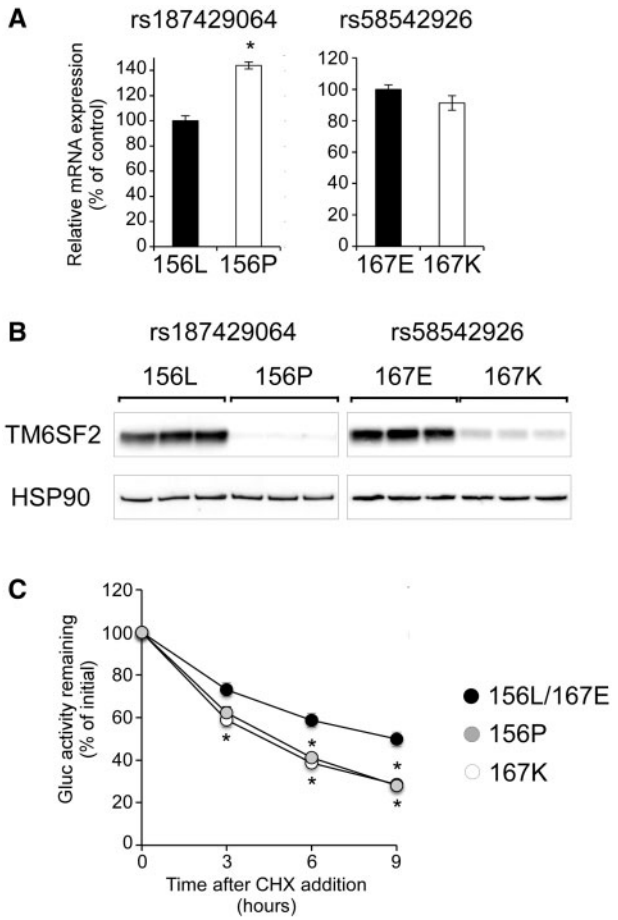

Figure 6. L156P and E167K variants reduce TM6SF2 protein expression by increasing rate of turnover. Huh7 cells stably expressing the 156P, 167K or 156L/167E (control) isoforms of V5-TM6SF2 were analyzed. (**A**) Relative mRNA expression of *TM6SF2* ($n = 3$ wells per group). (**B**) Western blot analysis of V5-TM6SF2 and HSP90. (**C**) Degradation of Gluc-TM6SF2 fusion proteins after treatment with cycloheximide (CHX, 10 μg/ml). Fractions of initial luciferase activity remaining are shown ($n = 6$ wells per group per time-point per experiment). Data are presented as the mean ± SEM of four to eight independent experiments. *$P < 0.05$ by ANOVA.

with the release of ApoB-lipoprotein particles from the organelle. ER-to-Golgi transport of ApoB-lipoproteins is mediated by a molecular machinery orchestrating the recruitment of pre-VLDL cargo to ER exit sites and packaging into specialized VLDL transport vesicles (VTV) (35). As Tm6sf2 is localized to the ER, ERGIC and Golgi (15,16), its overexpression may directly affect ER-to-Golgi trafficking of pre-VLDL particles. It is conceivable that Tm6sf2 interacts with a critical component of the protein complex mediating VTV assembly/release and titration of this component by excess Tm6sf2 may disrupt lipoprotein export from the ER. Consistent with a role in VLDL trafficking, TM6SF2 deficiency reduced APOB secretion in cultured human hepatocytes (16). In contrast, a recent report demonstrated that Tm6sf2 deficiency impairs the lipidation, but not secretion of ApoB-lipoprotein particles (15). The reason for discrepancy between the two studies is currently unclear. Thus, while both overexpression and deficiency of Tm6sf2 suppress VLDL-TG secretion (3,15), the underlying molecular mechanisms may be different. Collectively, these results implicate Tm6sf2 in the intracellular transport and lipidation of VLDL particles and may identify a previously unrecognized molecular link between these processes.

While investigating the metabolic role of Tm6sf2 in genetically engineered mouse models has been a primary focus of recent studies, the functional consequences of naturally occurring genetic variation in the human *TM6SF2* gene have not been fully explored. Genome- and exome-wide association studies identified two coding variants (L156P and E167K) in TM6SF2 to be independently associated with plasma lipids, NAFLD and alcohol-induced cirrhosis (2,3,5,8). We determined that rare alleles of both variants (i.e. P156 and K167) increased the rate of turnover and markedly reduced steady state cellular levels of TM6SF2. These results confirm that L256P and E167K are functional variants, and suggest that their association with plasma lipid levels and fatty liver disease is mediated by altered TM6SF2 protein expression. Furthermore, we demonstrate for the first time that the rare alleles of these polymorphisms represent loss-of-function variants. As P156 and K167 are associated with lower plasma lipid levels in humans, our results also indicate that loss of TM6SF2 function is the underlying mechanism; a conclusion consistent with mouse models of Tm6sf2 deficiency (3,15). Amino acid L156 is evolutionarily conserved among paralogous members of the EXPERA protein family (18) and located within one of the predicted helical transmembrane domains of TM6SF2. Thus, substitution of L156 with proline, a helix breaker, likely interferes with insertion of the domain into the membrane, alters overall TM6SF2 topology and leads to decreased stability and increased degradation of the protein. E167K is a charge-altering amino acid substitution, which may impair protein stability by altering overall protein structure. However, the closest homolog of TM6SF2, TM6SF1, harbors a positively charged residue (i.e. arginine) at position 167, which makes this explanation unlikely (18). Thus, we favor the alternative possibility that E167K disrupts interaction with another protein that is critically required for the stability of TM6SF2. Future studies will be required to explore this hypothesis. In conclusion, our results demonstrate that rs187429064 (L156P) and rs58542926 (E167K) are causative genetic variants and exert their effects on lipid metabolism at least in part through the modulation of TM6SF2 protein abundance.

In the present study, we demonstrated that elevated hepatic Tm6sf2 expression has significant impact on plasma lipoproteins, atherosclerosis and fatty liver disease. The observation that both excess and deficiency of Tm6sf2 lead to altered lipid metabolism indicates that the level of Tm6sf2 expression is an important determinant of metabolic homeostasis. Indeed, we have shown that SNPs associated with metabolic traits in human populations alter cellular TM6SF2 protein levels. An unexpected finding of our study is that Tm6sf2 overexpression resulted in metabolic phenotypes that have previously been observed in loss-of-function models. Deciphering the underlying mechanisms in future studies may shed new light on the molecular function and interactions of Tm6sf2 in the regulation of ApoB-lipoprotein metabolism.

Materials and Methods

Mice

C57BL/6J and Ldlr$^{-/-}$;ApoB$^{100/100}$ (referred to as DKO) mice were obtained from The Jackson Laboratory (stock #003000) and bred in-house. Animals were maintained on a 14-h light/10-h dark cycle and fed *ad libitum* Laboratory Rodent Diet 5053 (LabDiet), a high-fat diet (D12492; 60 kcal% from lard; Research Diets) or a HC diet (TD 88137; 0.2% cholesterol; Harlan Teklad) with free access to water. Unless otherwise noted, mice were fasted for 4 h (8:00 am to 12:00 pm) before blood collection. For overnight fasting, mice were deprived of food for 16 h (6:00 pm to 10:00 am).

All experimental procedures were approved by the Institutional Animal Care and Use Committees at Cedars-Sinai Medical Center and Western University.

AAV-mediated expression

Mouse and human *TM6SF2* coding cDNA sequences without epitope tag were used to replace eGFP in the pENN.AAV.TBG.PI.eGFP vector (p1014; Penn Vector Core), which drives expression from the TBG promoter. AAV serotype 8 (AAV8) particles were packaged and purified on a fee-for-service basis at the Penn Vector Core (Perelman School of Medicine, University of Pennsylvania). Empty (AAV-Null) or eGFP-expressing [AAV-green fluorescent protein (GFP)] vectors were used as controls. AAV8 particles were intravenously injected through the retro-orbital sinus at a dose of 10^{12} gc per mouse, unless otherwise noted.

Plasma and liver chemistries

For plasma lipid and lipoprotein analyses, blood was collected from mice after 4 h fasting. Plasma lipid levels were determined as described (36). To assess lipoprotein distribution, equal volumes of plasma from three to eight mice were pooled and analyzed by size fractionation on a FPLC column at the Mouse Metabolic Phenotyping Center at Vanderbilt University School of Medicine. Plasma ALT activity and bilirubin concentration were determined by colorimetric assays (Pointe Scientific and Sigma-Aldrich, respectively). Lipids were extracted from pieces of liver (50–100 mg) using the Folch method (37) followed by enzymatic analysis of TG, total cholesterol and free cholesterol, as described (38).

Hepatic TG secretion

After 4 h fasting, AAV-treated mice were intraperitoneally injected with 1 mg/g body weight of Pluronic F-127 (Sigma) to block vascular TG hydrolysis by lipoprotein lipase (39). Blood was obtained by retro-orbital bleeding before and 1 or 2 h after injection followed by analyses of TG and cholesterol (Amplex® Red Cholesterol Assay Kit, Thermo Fisher Scientific).

MTTP activity assay

Liver (~100 mg) or Huh7 cells grown in 6-well plates were homogenized and assayed using fluorescently labeled triglyceride substrate as described previously (40).

Assessment of atherosclerotic lesions

After 12 weeks of HC diet feeding, mice were anesthetized with isoflurane and the aorta and heart were excised. Aortas were excised from the aortic arch to the iliac bifurcation. *En face*-mounted aortas, aortic sinus and aortic arch sections were prepared and stained with ORO as previously described (41,42). Lesion and ORO-stained areas were quantified as described (43). As no differences between sexes were observed, data from male and female mice have been combined and analyzed together.

RNA analysis

mRNA levels were determined by real-time PCR analysis as described (44) using 36B4 as internal control. Primer sequences are available upon request.

Cell culture studies

Cellular lipoprotein metabolism was assessed in human hepatoma cell lines (Huh7, HepG2 and Hep3B) obtained from the American Type Culture Collection and grown under standard culture conditions. Primary human HLCs were derived by differentiating an iPSC line (83i-CTRL) established at the Cedars-Sinai Medical Center iPSC Core as described (45,46). Cell lines were periodically tested negative for mycoplasma contamination. To generate stable cell lines, a lentiviral vector (pFG.EF1.mCherry.IRES.Puro.WPRE) was used to express mCherry (mCh) or V5-TM6SF2 under the control of the EF1 promoter. Cell lines were maintained in media supplemented with 2 μg/ml puromycin. APOB secretion was assessed by incubating sub-confluent cells cultured in triplicate wells of 48-well plates for 4–6 h in fresh media. APOB secretion from Huh7 and HepG2 cells has previously been found to be linear for up to 24 h with no evidence of reuptake of secreted lipoproteins (16). APOB concentrations in cell culture media were quantitated using an ELISA kit (3715-1H-6; Mabtech) according to the manufacturer's instructions. To normalize for cell number and control for non-specific effects affecting secretion, albumin secretion was also determined (E80-129; Bethyl Laboratories) from an aliquot of the same samples.

For transient overexpression, Hep3B cells or HLCs were infected (MOI = 10–40) with adenoviral vectors expressing TM6SF2 or mCherry under control of the CMV promoter. APOB and albumin secretion assays were conducted 2 days after adenoviral transduction. Transduced Hep3B cells (three wells per condition) were treated with either BSA or a BSA:OA complex (1:5 molar ratio; 0.6 mM OA) for 8 h, lactacystin (Lacta, 10 μM; Sigma), 3-methyladenine (3-MA, 5 mM; Cayman Chemical) or vehicle (DMSO) for 4 h. After treatment, media were replaced with fresh media, which was then collected 4 h later for APOB/albumin analysis.

For the measurement of intracellular APOB, cells cultured in 6-well plates were rinsed in PBS and resuspended in lysis buffer (100 mM Tris–HCl, pH 7.4, 150 mM NaCl, 1 mM EGTA, 1 mM EDTA, 1% Triton X-100, 0.5% sodium deoxycholate, protease inhibitors). APOB in cell lysates was assayed with ELISA based on the 1D1 monoclonal antibody, which recognizes lipid-free and lipid-associated APOB with equal affinity (47).

Western blot analyses

To detect ApoB in liver, tissue samples were homogenized in a buffer containing 62 mM sucrose, 0.5% sodium deoxycholate, 0.5% Triton X-100, 5 mM EDTA, 50 mM Tris–HCl (pH 7.4), 150 mM NaCl (pH 7.4) and protease inhibitors. One hundred micrograms of liver lysates were fractionated by 6% SDS-PAGE followed by transfer to nitrocellulose membrane. Following blocking with 5% milk, membranes were incubated with a rabbit anti-mouse ApoB antibody (K23300R, Meridian Life Science; 1:1000 dilution) at 4°C overnight and Alexa Fluor 633-conjugated goat anti-rabbit IgG antibody (A-21070, ThermoFisher; 1:10 000 dilution) at room temperature for 1 h. Blots were visualized with a Storm 640 device (Amersham). For normalization of ApoB signal, blots were re-probed with monoclonal anti-vinculin antibody (Sigma V9131; 1:1000 dilution) and goat anti-mouse IgG antibody (A-21050, ThermoFisher; 1:10 000 dilution). Mouse plasma was similarly analyzed after SDS-PAGE separation of equal sample volumes representing 0.5 μl of plasma.

To detect V5 epitope-tagged TM6SF2 in Huh7 cells, cells cultured in six-well plates were lysed (10 mM Tris–HCl, pH 7.4, 150 mM NaCl, 1% NP40, protease inhibitors), separated by 10% SDS-PAGE and transferred to PVDF membrane. After blocking,

membranes were probed with mouse monoclonal anti-V5 (R960-25, ThermoFisher; 1:10 000 dilution) and HRP-conjugated rabbit anti-mouse IgG (315-035-003, Jackson ImmunoResearch; 1:100 000 dilution) antibodies. For normalization, membranes were re-probed with rabbit anti-HSP90 (sc-7947, Santa Cruz Biotechnology; 1:1000 dilution) and HRP-conjugated donkey anti-rabbit IgG (711-035-152, Jackson ImmunoResearch; 1:100 000 dilution) antibodies. Bands were visualized using the SuperSignal West Femto chemiluminescent substrate (ThermoFisher).

Subcellular localization of APOB

Huh7 cells transduced with either empty (LV-Null) or V5-TM6SF2 expressing lentivirus (LV-TM6SF2) were plated on poly-D-lysine coated glass coverslips and fixed with 4% paraformaldehyde for 10 min. Cells were permeabilized with 0.2% Triton X-100 for 10 min and blocked with 10% goat serum and 10% donkey serum for 30 min. Cells were then stained with a monoclonal mouse anti-human APOB mAbs (LDL 20/17, Mabtech; 1:500 dilution) and rabbit anti-CRT antibody (SPA-600, Stressgen; 1:500) for 1 h at room temperature. Secondary antibody staining was done with Cy3-conjugated goat anti-mouse IgG (115-165-003, Jackson ImmunoResearch; 1:500) and Alexa Fluor 488-conjugated goat anti-rabbit IgG (111-545-003, Jackson ImmunoResearch; 1:1000) for 1 h at room temperature. Cells were then stained with DAPI for 5 min. Coverslips were mounted on microscope slides with Vectashield mounting medium. Images were taken using a Leica SP5-X confocal microscope. The Colocalization Quantification Tool in the Leica Application Suite Advanced Fluorescence (version 2.6) software application was used to determine co-localization rates.

Measurement of TM6SF2 turnover rate

To assess the impact of TM6SF2 coding polymorphisms on rate of degradation, we generated an in-frame fusion construct between Gaussia luciferase and TM6SF2 (Gluc-TM6SF2) representing the common alleles (*i.e.* 156L and 167E) of rs187429064 and rs58542926. Constructs carrying the minor alleles (*i.e.* 156P and 167K) were generated by site-directed mutagenesis. Huh7 cell lines stably expressing the major and minor Gluc-TM6SF2 isoforms (156L/167E, 156P/167E and 156L/167K) were generated by lentiviral transduction and cultured in the presence of 2 μg/ml puromycin. Cells were grown to confluency in 48-well plates and the next day sextuplicate wells were treated with vehicle (DMSO) or 10 μg/ml CHX for 3, 6 or 9 h. After cell lysis in Passive Lysis buffer (E1941, Promega), luciferase activity was assayed with the Gaussia Luciferase Assay Reagent (GAR-1, Targeting Systems).

Supplementary Material

Supplementary Material is available at *HMG* online.

Acknowledgements

We thank Kolja Wawrowsky, Dieu-Trang (Sandrine) Fuchs and John Burke for expert technical assistance.

Conflict of Interest statement. None declared.

Funding

This work was supported in whole or part by the National Institutes of Health [P01 HL028481], [NCRR UL1RR033176] to M.P.; [T32 DK007770] to M.E.D.; [R01 HL111483] to S.C.; and [U24 DK059637] to the MMPC at Vanderbilt University School of Medicine.

References

1. Global Lipids Genetics Consortium, Willer, C.J., Schmidt, E.M., Sengupta, S., Peloso, G.M., Gustafsson, S., Kanoni, S., Ganna, A., Chen, J., Buchkovich, M.L. *et al*. (2013) Discovery and refinement of loci associated with lipid levels. *Nat. Genet.*, **45**, 1274–1283.
2. Holmen, O.L., Zhang, H., Fan, Y., Hovelson, D.H., Schmidt, E.M., Zhou, W., Guo, Y., Zhang, J., Langhammer, A., Lochen, M.L. *et al*. (2014) Systematic evaluation of coding variation identifies a candidate causal variant in TM6SF2 influencing total cholesterol and myocardial infarction risk. *Nat. Genet.*, **46**, 345–351.
3. Kozlitina, J., Smagris, E., Stender, S., Nordestgaard, B.G., Zhou, H.H., Tybjaerg-Hansen, A., Vogt, T.F., Hobbs, H.H. and Cohen, J.C. (2014) Exome-wide association study identifies a TM6SF2 variant that confers susceptibility to nonalcoholic fatty liver disease. *Nat. Genet.*, **46**, 352–356.
4. Saxena, R., Elbers, C.C., Guo, Y., Peter, I., Gaunt, T.R., Mega, J.L., Lanktree, M.B., Tare, A., Castillo, B.A., Li, Y.R. *et al*. (2012) Large-scale gene-centric meta-analysis across 39 studies identifies type 2 diabetes loci. *Am. J. Hum. Genet.*, **90**, 410–425.
5. Surakka, I., Horikoshi, M., Magi, R., Sarin, A.P., Mahajan, A., Lagou, V., Marullo, L., Ferreira, T., Miraglio, B., Timonen, S. *et al*. (2015) The impact of low-frequency and rare variants on lipid levels. *Nat. Genet.*, **47**, 589–597.
6. Teslovich, T.M., Musunuru, K., Smith, A.V., Edmondson, A.C., Stylianou, I.M., Koseki, M., Pirruccello, J.P., Ripatti, S., Chasman, D.I., Willer, C.J. *et al*. (2010) Biological, clinical and population relevance of 95 loci for blood lipids. *Nature*, **466**, 707–713.
7. Willer, C.J., Sanna, S., Jackson, A.U., Scuteri, A., Bonnycastle, L.L., Clarke, R., Heath, S.C., Timpson, N.J., Najjar, S.S., Stringham, H.M. *et al*. (2008) Newly identified loci that influence lipid concentrations and risk of coronary artery disease. *Nat. Genet.*, **40**, 161–169.
8. Buch, S., Stickel, F., Trepo, E., Way, M., Herrmann, A., Nischalke, H.D., Brosch, M., Rosendahl, J., Berg, T., Ridinger, M. *et al*. (2015) A genome-wide association study confirms PNPLA3 and identifies TM6SF2 and MBOAT7 as risk loci for alcohol-related cirrhosis. *Nat. Genet.*, **47**, 1443–1448.
9. O'Hare, E.A., Yang, R., Yerges-Armstrong, L., Sreenivasan, U., McFarland, R., Leitch, C.C., Wilson, M.H., Narina, S., Gorden, A., Ryan, K. *et al*. (2017) TM6SF2 rs58542926 impacts lipid processing in liver and small intestine. *Hepatology*, **65**, 1526–1542.
10. Dongiovanni, P., Petta, S., Maglio, C., Fracanzani, A.L., Pipitone, R., Mozzi, E., Motta, B.M., Kaminska, D., Rametta, R., Grimaudo, S. *et al*. (2015) TM6SF2 gene variant disentangles nonalcoholic steatohepatitis from cardiovascular disease. *Hepatology*, **61**, 506–514.
11. Falleti, E., Cussigh, A., Cmet, S., Fabris, C. and Toniutto, P. (2016) PNPLA3 rs738409 and TM6SF2 rs58542926 variants increase the risk of hepatocellular carcinoma in alcoholic cirrhosis. *Dig. Liver Dis.*, **48**, 69–75.

12. Liu, Y.L., Reeves, H.L., Burt, A.D., Tiniakos, D., McPherson, S., Leathart, J.B., Allison, M.E., Alexander, G.J., Piguet, A.C., Anty, R. *et al.* (2014) TM6SF2 rs58542926 influences hepatic fibrosis progression in patients with non-alcoholic fatty liver disease. *Nat. Commun.*, **5**, 4309.
13. Sookoian, S., Castano, G.O., Scian, R., Mallardi, P., Fernandez Gianotti, T., Burgueno, A.L., San Martino, J. and Pirola, C.J. (2015) Genetic variation in transmembrane 6 superfamily member 2 and the risk of nonalcoholic fatty liver disease and histological disease severity. *Hepatology*, **61**, 515–525.
14. Sookoian, S. and Pirola, C.J. (2016) Meta-analysis of the influence of TM6SF2 E167K variant on plasma concentration of aminotransferases across different populations and diverse liver phenotypes. *Sci. Rep.*, **6**, 27718.
15. Smagris, E., Gilyard, S., BasuRay, S., Cohen, J.C. and Hobbs, H.H. (2016) Inactivation of Tm6sf2, a gene defective in fatty liver disease, impairs lipidation but not secretion of very low density lipoproteins. *J. Biol. Chem.*, **291**, 10659–10676.
16. Mahdessian, H., Taxiarchis, A., Popov, S., Silveira, A., Franco-Cereceda, A., Hamsten, A., Eriksson, P. and Van't Hooft, F. (2014) TM6SF2 is a regulator of liver fat metabolism influencing triglyceride secretion and hepatic lipid droplet content. *Proc. Natl. Acad. Sci. U. S. A.*, **111**, 8913–8918.
17. Fan, Y., Lu, H., Guo, Y., Zhu, T., Garcia-Barrio, M.T., Jiang, Z., Willer, C.J., Zhang, J. and Chen, Y.E. (2016) Hepatic transmembrane 6 superfamily member 2 regulates cholesterol metabolism in mice. *Gastroenterology*, **150**, 1208–1218.
18. Sanchez-Pulido, L. and Ponting, C.P. (2014) TM6SF2 and MAC30, new enzyme homologs in sterol metabolism and common metabolic disease. *Front. Genet.*, **5**, 439.
19. Kassim, S.H., Li, H., Vandenberghe, L.H., Hinderer, C., Bell, P., Marchadier, D., Wilson, A., Cromley, D., Redon, V., Yu, H. *et al.* (2010) Gene therapy in a humanized mouse model of familial hypercholesterolemia leads to marked regression of atherosclerosis. *PLoS One*, **5**, e13424.
20. Veniant, M.M., Sullivan, M.A., Kim, S.K., Ambroziak, P., Chu, A., Wilson, M.D., Hellerstein, M.K., Rudel, L.L., Walzem, R.L. and Young, S.G. (2000) Defining the atherogenicity of large and small lipoproteins containing apolipoprotein B100. *J. Clin. Invest.*, **106**, 1501–1510.
21. Meex, S.J., Andreo, U., Sparks, J.D. and Fisher, E.A. (2011) Huh-7 or HepG2 cells: which is the better model for studying human apolipoprotein-B100 assembly and secretion? *J. Lipid Res.*, **52**, 152–158.
22. Butkinaree, C., Guo, L., Ramkhelawon, B., Wanschel, A., Brodsky, J.L., Moore, K.J. and Fisher, E.A. (2014) A regulator of secretory vesicle size, Kelch-like protein 12, facilitates the secretion of apolipoprotein B100 and very-low-density lipoproteins—brief report. *Arterioscler. Thromb. Vasc. Biol.*, **34**, 251–254.
23. Gusarova, V., Brodsky, J.L. and Fisher, E.A. (2003) Apolipoprotein B100 exit from the endoplasmic reticulum (ER) is COPII-dependent, and its lipidation to very low density lipoprotein occurs post-ER. *J. Biol. Chem.*, **278**, 48051–48058.
24. Prelich, G. (2012) Gene overexpression: uses, mechanisms, and interpretation. *Genetics*, **190**, 841–854.
25. Wang, P., Zhou, Z., Hu, A., Ponte de Albuquerque, C., Zhou, Y., Hong, L., Sierecki, E., Ajiro, M., Kruhlak, M., Harris, C. *et al.* (2014) Both decreased and increased SRPK1 levels promote cancer by interfering with PHLPP-mediated dephosphorylation of Akt. *Mol. Cell*, **54**, 378–391.
26. Eisenberg, S. (1984) High density lipoprotein metabolism. *J. Lipid Res.*, **25**, 1017–1058.
27. Strauss, J.G., Frank, S., Kratky, D., Hammerle, G., Hrzenjak, A., Knipping, G., von Eckardstein, A., Kostner, G.M. and Zechner, R. (2001) Adenovirus-mediated rescue of lipoprotein lipase-deficient mice. Lipolysis of triglyceride-rich lipoproteins is essential for high density lipoprotein maturation in mice. *J. Biol. Chem.*, **276**, 36083–36090.
28. Khovidhunkit, W., Kim, M.S., Memon, R.A., Shigenaga, J.K., Moser, A.H., Feingold, K.R. and Grunfeld, C. (2004) Effects of infection and inflammation on lipid and lipoprotein metabolism: mechanisms and consequences to the host. *J. Lipid Res.*, **45**, 1169–1196.
29. Bieghs, V., Vlassaks, E., Custers, A., van Gorp, P.J., Gijbels, M.J., Bast, A., Bekers, O., Zimmermann, L.J., Lutjohann, D., Voncken, J.W. *et al.* (2010) Chorioamnionitis induced hepatic inflammation and disturbed lipid metabolism in fetal sheep. *Pediatr. Res.*, **68**, 466–472.
30. Dichek, H.L., Johnson, S.M., Akeefe, H., Lo, G.T., Sage, E., Yap, C.E. and Mahley, R.W. (2001) Hepatic lipase overexpression lowers remnant and LDL levels by a noncatalytic mechanism in LDL receptor-deficient mice. *J. Lipid Res*, **42**, 201–210.
31. MacArthur, J.M., Bishop, J.R., Stanford, K.I., Wang, L., Bensadoun, A., Witztum, J.L. and Esko, J.D. (2007) Liver heparan sulfate proteoglycans mediate clearance of triglyceride-rich lipoproteins independently of LDL receptor family members. *J. Clin. Invest.*, **117**, 153–164.
32. Rohlmann, A., Gotthardt, M., Hammer, R.E. and Herz, J. (1998) Inducible inactivation of hepatic LRP gene by cre-mediated recombination confirms role of LRP in clearance of chylomicron remnants. *J. Clin. Invest.*, **101**, 689–695.
33. Fisher, E.A. (2012) The degradation of apolipoprotein B100: multiple opportunities to regulate VLDL triglyceride production by different proteolytic pathways. *Biochim. Biophys. Acta*, **1821**, 778–781.
34. Ginsberg, H.N. and Fisher, E.A. (2009) The ever-expanding role of degradation in the regulation of apolipoprotein B metabolism. *J. Lipid Res.*, **50(Suppl)**, S162–S166.
35. Tiwari, S. and Siddiqi, S.A. (2012) Intracellular trafficking and secretion of VLDL. *Arterioscler. Thromb. Vasc. Biol.*, **32**, 1079–1086.
36. Hosseini, M., Ehrhardt, N., Weissglas-Volkov, D., Lai, C.M., Mao, H.Z., Liao, J.L., Nikkola, E., Bensadoun, A., Taskinen, M.R., Doolittle, M.H. *et al.* (2012) Transgenic expression and genetic variation of Lmf1 affect LPL activity in mice and humans. *Arterioscler. Thromb. Vasc. Biol.*, **32**, 1204–1210.
37. Folch, J., Lees, M. and Sloane Stanley, G.H. (1957) A simple method for the isolation and purification of total lipides from animal tissues. *J. Biol. Chem.*, **226**, 497–509.
38. Carr, T.P., Andresen, C.J. and Rudel, L.L. (1993) Enzymatic determination of triglyceride, free cholesterol, and total cholesterol in tissue lipid extracts. *Clin. Biochem.*, **26**, 39–42.
39. Millar, J.S., Cromley, D.A., McCoy, M.G., Rader, D.J. and Billheimer, J.T. (2005) Determining hepatic triglyceride production in mice: comparison of poloxamer 407 with Triton WR-1339. *J. Lipid Res.*, **46**, 2023–2028.
40. Soh, J., Iqbal, J., Queiroz, J., Fernandez-Hernando, C. and Hussain, M.M. (2013) MicroRNA-30c reduces hyperlipidemia and atherosclerosis in mice by decreasing lipid synthesis and lipoprotein secretion. *Nat. Med.*, **19**, 892–900.
41. Michelsen, K.S., Wong, M.H., Shah, P.K., Zhang, W., Yano, J., Doherty, T.M., Akira, S., Rajavashisth, T.B. and Arditi, M. (2004) Lack of Toll-like receptor 4 or myeloid differentiation factor 88 reduces atherosclerosis and alters plaque phenotype in mice deficient in apolipoprotein E. *Proc. Natl. Acad. Sci. U. S. A.*, **101**, 10679–10684.

42. Naiki, Y., Sorrentino, R., Wong, M.H., Michelsen, K.S., Shimada, K., Chen, S., Yilmaz, A., Slepenkin, A., Schroder, N.W., Crother, T.R. *et al.* (2008) TLR/MyD88 and liver X receptor alpha signaling pathways reciprocally control Chlamydia pneumoniae-induced acceleration of atherosclerosis. *J. Immunol.*, **181**, 7176–7185.
43. Chen, S., Lee, Y., Crother, T.R., Fishbein, M., Zhang, W., Yilmaz, A., Shimada, K., Schulte, D.J., Lehman, T.J., Shah, P.K. *et al.* (2012) Marked acceleration of atherosclerosis after Lactobacillus casei-induced coronary arteritis in a mouse model of Kawasaki disease. *Arterioscler. Thromb. Vasc. Biol.*, **32**, e60–e71.
44. Mao, H.Z., Ehrhardt, N., Bedoya, C., Gomez, J.A., DeZwaan-McCabe, D., Mungrue, I.N., Kaufman, R.J., Rutkowski, D.T. and Peterfy, M. (2014) Lipase maturation factor 1 (lmf1) is induced by endoplasmic reticulum stress through activating transcription factor 6α (Atf6α) signaling. *J. Biol. Chem.*, **289**, 24417–24427.
45. Hatada, S., Subramanian, A., Mandefro, B., Ren, S., Kim, H.W., Tang, J., Funari, V., Baloh, R.H., Sareen, D., Arumugaswami, V. *et al.* (2015) Low-dose irradiation enhances gene targeting in human pluripotent stem cells. *Stem Cells Transl. Med.*, **4**, 998–1010.
46. Ignatius Irudayam, J., Contreras, D., Spurka, L., Subramanian, A., Allen, J., Ren, S., Kanagavel, V., Nguyen, Q., Ramaiah, A., Ramamoorthy, K. *et al.* (2015) Characterization of type I interferon pathway during hepatic differentiation of human pluripotent stem cells and hepatitis C virus infection. *Stem Cell Res.*, **15**, 354–364.
47. Bakillah, A., Zhou, Z., Luchoomun, J. and Hussain, M.M. (1997) Measurement of apolipoprotein B in various cell lines: correlation between intracellular levels and rates of secretion. *Lipids*, **32**, 1113–1118.